Infrared Image Enhancement in Maritime Environment with Convolutional Neural Networks

Purbaditya Bhattacharya[1], Jörg Riechen[2] and Udo Zölzer[1]
[1]*Department of Signal Processing and Communications, Helmut Schmidt University, Hamburg, Germany*
[2]*WTD 71 Military Service Center for Ships, Naval Weapons, Maritime Technology and Research, Eckernförde, Germany*

Keywords: Image Processing, Convolutional Neural Network, Denoising, Super-resolution.

Abstract: Image enhancement approach with Convolutional Neural Network (CNN) for infrared (IR) images from maritime environment, is proposed in this paper. The approach includes different CNNs to improve the resolution and to reduce noise artefacts in maritime IR images. The denoising CNN employs a residual architecture which is trained to reduce graininess and fixed pattern noise. The super-resolution CNN employs a similar architecture to learn the mapping from a low-resolution to multi-scale high-resolution images. The performance of the CNNs is evaluated on the IR test dataset with standard evaluation methods and the evaluation results show an overall improvement in the quality of the IR images.

1 INTRODUCTION

Optical cameras contain sensors that are able to detect light of wavelength in the range of 450 - 750 nm and hence limited by the availability of light. Infrared (IR) cameras and thermographic cameras in particular have sensors that detect thermal radiation and are independent from the amount of ambient visible light. The thermal radiation of the object determines how salient or detailed it will be in an infrared image and can provide useful information, otherwise not available in a normal image. IR imagery has become considerably popular over the last years because of its usage in multiple fields of application including medical imaging, material testing, military surveillance. Due to its effectiveness, IR imaging is used extensively in maritime environment for maritime safety and security application, activity detection, object tracking, and environment monitoring.

(a) Original (b) Enhanced

Figure 1: An example of enhancement in IR images.

IR images suffer from low signal-to-noise ratio (SNR) because of the non-uniformity of the detector array responses and their underlying processing circuits. The ambient temperature plays a very important role since the IR camera has to be calibrated accordingly (Zhang et al., 2010). In this context, outdoor maritime environment poses a bigger challenge compared to an indoor environment due to the temperature fluctuations, atmospheric loss, wind, and rain. In spite of regular camera calibrations and error correcting techniques (Zhang et al., 2010), the image suffers from spot noise, fixed pattern noise, graininess, blur and other artefacts. Traditional digital image processing techniques of image enhancement have been extensively used over the years. The classical approaches include the usage of adaptive median filters, gradient based approach like the total variation denoising (Micchelli et al., 2011), (Goldstein and Osher, 2009), wavelet based approach (Zhou et al., 2009), non-local self similarity (NSS) based methods (Dabov et al., 2007), (J.Xu et al., 2015), and methods on sparse representation based dictionary learning

Bhattacharya, P., Riechen, J. and Zölzer, U.
Infrared Image Enhancement in Maritime Environment with Convolutional Neural Networks.
DOI: 10.5220/0006618700370046
In *Proceedings of the 13th International Joint Conference on Computer Vision, Imaging and Computer Graphics Theory and Applications (VISIGRAPP 2018) - Volume 4: VISAPP*, pages 37-46
ISBN: 978-989-758-290-5

(Elad and Aharon, 2006). In recent years deep learning has become a very popular topic due to its success in solving many computer vision problems. Convolutional neural network (CNN) is the most popular deep learning tool and has been employed already in many image enhancement problems e.g., denoising, super-resolution, and compression artefact removal. This paper applies a deep learning approach with CNNs to solve the enhancement problem in maritime IR images. An example is shown in Figure 1.

2 RELATED WORK

The present work is influenced by the recent success of CNNs in image super-resolution and denoising problems. An artificial neural network is used for image denoising in (Jain and Seung, 2009). It is shown in (Burger et al., 2012) that multi layer perceptrons (MLP) can outperform state-of-the-art standard denoising techniques. In the area of resolution improvement, the ”Super-Resolution Convolutional Neural Network” (SRCNN) (Dong et al., 2015) has trained a CNN architecture to learn the mapping between a low and high resolution image. The end to end learning has yielded very good results but the corresponding training convergence is slow. In (He et al., 2016) it is already established that residual connections or skip connections in a network increase the learning speed and improve the overall performance. Residual networks are particularly useful if the training data and the ground truth data have high correlation. In this context, CNNs with residual learning has yielded better results from the perspective of speed and accuracy. In (Kim et al., 2016) it is established that the super-resolution with a deep residual architecture subsequently improved the performance. Recently residual learning for image denoising with CNNs have been used successfully in (Pan et al., 2016) and (Zhang et al., 2017). Due to the improved performance of residual networks the present work has employed residual architectures for the enhancement application.

3 PROPOSED APPROACH

A CNN is a layered architecture primarily comprising of linear multi dimensional convolution kernels and non-linear activation functions usually appearing alternately in a basic architecture. Apart from the two layers mentioned, other important layers include pooling, batch normalization, and fully connected layers and the usage of these layers depends

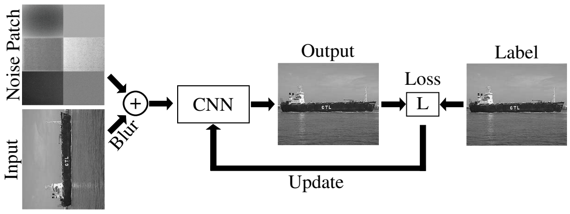

Figure 2: An overview of the denoising method.

on the computer vision application. The layers are arranged in different combinations to create flexible network architectures that are trained iteratively with an objective function to solve different computer vision problems. In order to perform a supervised training of a CNN, it is necessary to create a dataset of image and ground truth pairs. The purpose of the training is to learn and generalize the relationship between the images and the corresponding ground truth images in the dataset. The dataset is usually divided into training, validation and test data. The final goal of a trained CNN is to perform the desired action on an unseen test data. The following sections provide the details of the denoising and super-resolution CNNs.

3.1 Denoising Method

The denoising method overview is shown in Figure 2. In the first step the dataset is prepared for the denoising task. The primary goal of this work is to successfully denoise the IR images from the WTD 71 dataset. For training the CNN the RGB-NIR scene database (Brown and Süsstrunk, 2011) from the EPFL Lausanne is used. The database contains a collection of near infrared (NIR) and color images of indoor and outdoor scenes from which the NIR images are used for training. In the second step the CNN is described, setup and trained.

3.1.1 Data Preparation

Figure 3: Sample clean images from the RGB-NIR training dataset.

From the RGB-NIR database 400 images and 60 images are selected for training and validation respectively. To create the training and validation dataset the clean NIR images are initially resampled and degraded with noise to create the input dataset for the

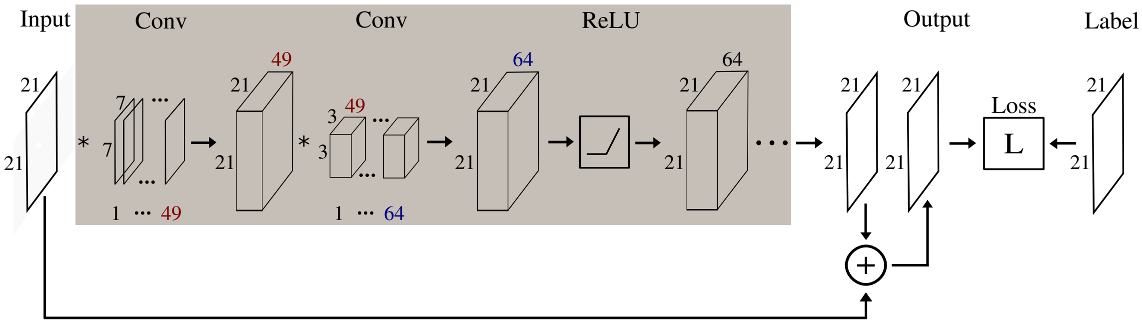

Figure 4: The architecture of denoising CNN.

CNN, and the clean NIR images are used as the ground truth or reference dataset. Figure 3 shows some example images from the database. A majority of the test IR images from WTD 71 have noisy artefacts of varying intensities and properties. A considerable number of noise patches are extracted from the IR images from areas of uniform background intensities. Additionally, noisy frames from videos with uniform background, containing 35 mm film grain, are extracted and added to the collection of noise patches. During the creation of the CNN dataset, the noise patches are randomly augmented and are added to the clean images after mean subtraction and resizing to produce the noisy images. The image and ground truth image pairs of both training and validation data are divided into patches of 21×21 pixels to create the final dataset. During the training process the image patches are randomly flipped.

3.1.2 Network Architecture

The example architecture for denoising is shown in Figure 4. As illustrated in the figure, the network is composed of alternate convolutional (Conv) layers and rectified linear units (ReLU), with the exception of the first two layers which are convolutional. The network is only composed of Conv layers and ReLU layers. There are 7 Conv layers and 5 ReLU layers in the network and 13 layers altogether including the Loss layer. The Conv layer performs linear convolution on each incoming feature map tensor or a tensor of input image patch with the defined kernels to produce the output feature maps. As shown in Figure 4 the depth of the convolution kernel should match the depth of the input feature map and the depth of the output feature map tensor is equal to the number of kernels in the Conv layer. Hence the number of kernels used in the final Conv layer should be 1 in order to obtain a target output image with a depth or channel of 1. The convolution operation in each Conv layer also retains the height and the width of the input feature map to that layer by correct padding. The depth of the convolution kernel is equal to the depth of the input feature map tensor. Thus a convolution of a 21×21×1 image patch with 49 kernels of size 7×7×1 produces a feature map tensor of size 21×21×49 in the first layer. The first two Conv layers use 7×7×1 and 3×3×49 kernels respectively and the last Conv layer uses 3×3×64 kernel. The kernels in the first Conv layer are initialized with sparse matrices where most of the elements are zero valued and the remaining elements have a value of 1. The remaining Conv layers use 5×5×64 kernels with ReLU layers in between. The ReLU layer truncates the negative values in a feature map as given by,

$$y = max(0,x), \tag{1}$$

where x denotes the input to the ReLU function, y denotes the output of the ReLU function, and max denotes the maximum operator. Before the Loss layer the input is added to the output so that the network learns to estimate the noise residue. Table 1 shows the information about the network architecture, where Id. denotes the layer index, and w and b denote weight and bias respectively. The table also provides the size of each kernel in the form of height×width×depth×number of kernels. The leakage factor (Lk) of the ReLU layer weights the negative values from the input feature maps instead of truncating them.

3.1.3 Objective

The objective of the training process is to minimize a combination of losses defined by the corresponding loss functions. The CNN is trained iteratively to minimize a weighted combination of loss functions in order to find an optimal solution of the free or trainable parameters. The combination consists of the L_1 and L_2 regression loss functions which operate pixel wise. The individual loss functions are given in the below equations,

$$L_1(y,\hat{y}) = \frac{1}{V}||y-\hat{y}||_1, \tag{2}$$

Table 1: The denoising CNN architecture.

Id.	Name	Kernel Size	Lk	lr (w, b)
1	Conv	7×7×1×49	-	1e-4, 1e-4
2	Conv	3×3×49×64	-	1e-2, 1e-4
3	ReLU	-	0.2	-
4	Conv	5×5×64×64	-	1e-2, 1e-4
5	ReLU	-	0.2	-
6	Conv	5×5×64×64	-	1e-2, 1e-4
7	ReLU	-	0.2	-
8	Conv	5×5×64×64	-	1e-2, 1e-4
9	ReLU	-	0.2	-
10	Conv	5×5×64×64	-	1e-2, 1e-4
11	ReLU	-	0.2	-
12	Conv	3×3×64×1	-	1e-2, 1e-4
13	Loss	-	-	-

and

$$L_2(y,\hat{y}) = \frac{1}{V}||y-\hat{y}||_2^2, \tag{3}$$

where $\hat{y}$ denotes the estimated CNN output, y denotes the ground truth data, and V denotes the volume of the CNN output or the ground truth data tensor. The advantage of the L_1 loss is that it has edge preserving qualities since the L_1 norm solves for the median. The optimization problem is given by,

$$\hat{y} = f_\theta(x), \tag{4}$$

$$\theta^* = arg\ min\ E_{y,\hat{y}}[\sum_{i=1}^{K} \alpha_i L_i(y,\hat{y}))], \tag{5}$$

where, θ^* denotes the optimal solution of the free or trainable parameters denoted by θ, f_θ denotes the CNN model, x denotes the input image, $L_i(\cdot)$ denotes a loss function, α_i is the weighting factor for combining the K loss functions, and $E_{y,\hat{y}}[\cdot]$ denotes the expected value of the combination of loss functions. From the loss layer the gradients starts backpropagating through each layer following the chain rule of derivatives. The kernel weights are then updated with the calculated gradients for the corresponding layers and the amount of update is controlled by a user specified learning rate parameter. In order to update the weights, the adaptive momentum (Adam) optimization (Kingma and Ba, 2014) is used, due to its fast convergence. The weights of the Conv layers are initialized with Xavier initialization (Glorot and Bengio, 2010) and the weight decay regularization parameter of 0.001 is used to counter overfitting problems. It is noteworthy that a CNN is usually not trained with one image per iteration but with a batch of images as determined by a user specified batch size. Images inside a batch are randomly selected from the entire dataset which leads to the stochastic nature of the training process. In this case a batch size of 64 is used during the training. During the training process, the learning rates as shown in Table 1 are adapted by reducing them by a factor of 2 at every 10th epoch. The network is trained for 90 epochs.

3.2 Super-resolution Method

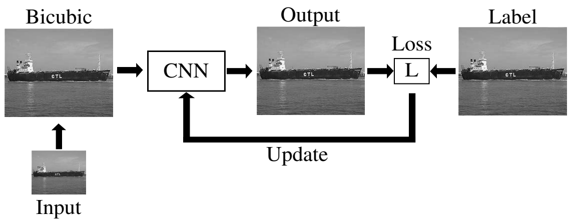

Figure 5: An overview of the super-resolution method.

In this section the CNN model for super-resolution is described. For super-resolution the RGB-NIR dataset is used as well. The method overview is shown in Figure 5. The model for the super-resolution CNN has differences from the denoising CNN in terms of the network architecture and data preparation.

3.2.1 Data Preparation

The dataset is prepared with 360 training images and 60 validation images. The training is performed with both the NIR images as well as with the Y channel of the color images converted to YCbCr, with the results from the latter being discussed in this work because of more stable performance. To create the training and validation dataset the clean images are initially resampled with bicubic interpolation to create the input dataset for the CNN and the clean images are used as the ground truth data. The CNN is trained with resampling factors of 2, 3, and 4 separately. The image and ground truth pairs of both training and validation data are divided into patches of 224×224 pixels to create the final dataset. During the training process the image patches are randomly flipped as a form of batch augmentation.

3.2.2 Network Architecture

The CNN architecture example for super-resolution is shown in Figure 6. The network is primarily composed of alternate Conv and ReLU layers and a concatenation (Concat) layer. The network has 13 Conv layers, 12 ReLU layers, 1 Concat layer, and has 27 layers in total including the Loss layer. Each Conv layer uses 3×3×64 kernel except the first layer which uses a 5×5×1 kernel and the layer after the Concat

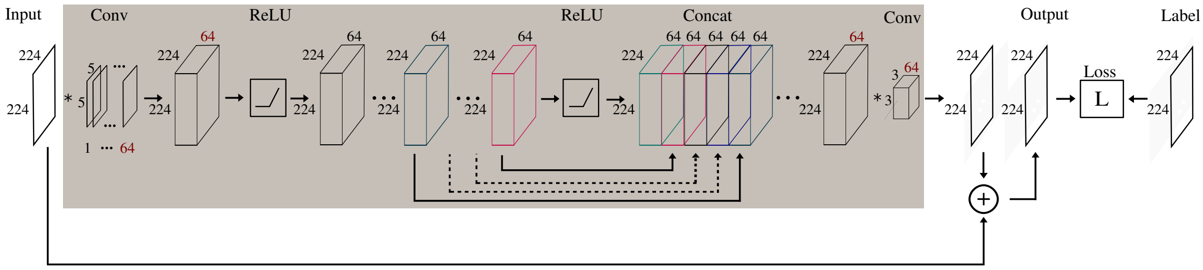

Figure 6: The architecture of super-resolution CNN.

layer which uses 5×5×320 kernel. All the layers employ 64 The learning rate (lr) of the Conv layers is the same. Before the last 2 Conv layers there is a Concat layer that collects feature maps from selected layers along the 3rd dimension of the feature tensor, as shown in Figure 6. In this particular case the feature maps from layers 6, 10, 14, 18, and 22, of a depth of 64 each, are concatenated along the 3rd dimension of the feature tensor resulting in a feature tensor with a depth of 320. The Concat layer ensures that the inference be made from feature maps from layers of multiple depths and hence multiple resolution with respect to the information content. The original image is added to the output by a skip connection and the network learns to estimate the residual high frequency details of the image. Table 2 shows the information about the network architecture. As mentioned previously the depth of the kernel in each Conv layer equals the depth of the corresponding input feature map. Hence, the kernel depth in the Conv layer following the Concat layer is 320 as given in Table 2. For super-resolution factors of 3 and 4, the same network architecture with different kernel depths (32), is used.

3.2.3 Objective

The super-resolution CNN is trained with a similar combination of loss functions as in the case of denoising. The goal of the training is to minimize the expected combined loss as given in Equation (5). The weights of the Conv layers are initialized with the improved Xavier initialization. The weight decay regularization parameter of 0.0005 is used and a batch size of 8 is used during training. The Adam optimizer is used to update the weights and biases in the Conv layers. During the training, the learning rate is adapted by reducing it by a factor of 2 after every 20th epoch. Training of the network with different resampling factors are performed separately for 230 epochs.

Table 2: The super-resolution CNN architecture.

Id.	Name	Kernel Size	Lk	lr (w, b)
1	Conv	5×5×1×64	-	1e-2, 1e-5
2	ReLU	-	0	-
3	Conv	3×3×64×64	-	1e-2, 1e-5
4	ReLU	-	0	-
5	Conv	3×3×64×64	-	1e-2, 1e-5
6	ReLU	-	0	-
7	Conv	3×3×64×64	-	1e-2, 1e-5
8	ReLU	-	0	-
9	Conv	3×3×64×64	-	1e-2, 1e-5
10	ReLU	-	0	-
11	Conv	3×3×64×64	-	1e-2, 1e-5
12	ReLU	-	0	-
13	Conv	3×3×64×64	-	1e-2, 1e-5
14	ReLU	-	0	-
15	Conv	3×3×64×64	-	1e-2, 1e-5
16	ReLU	-	0	-
17	Conv	3×3×64×64	-	1e-2, 1e-5
18	ReLU	-	0	-
19	Conv	3×3×64×64	-	1e-2, 1e-5
20	ReLU	-	0	-
21	Conv	3×3×64×64	-	1e-2, 1e-5
22	ReLU	-	0	-
23	Concat	-	-	-
24	Conv	3×3×320×64	-	1e-2, 1e-5
25	ReLU	-	0	-
26	Conv	3×3×64×1	-	1e-2, 1e-5
27	Loss	-	-	-

4 EVALUATION

The training of the CNNs are performed in MATLAB with the MatConvNet toolbox (Vedaldi and Lenc, 2015) on one Nvidia GTX 980Ti GPU. Training the individual networks took only a few hours. The performance of the networks are evaluated with the IR images from WTD 71. For evaluation of the quality of denoising and super-resolution, relatively clean images are selected from the database and are corrupted with film grain of 35 mm and fixed pattern noise. Some of the images from the dataset are shown in Figure 7. The results are also compared with established denoising methods BM3D (Dabov et al., 2007) and PGPD (J.Xu et al., 2015) and the DnCNN (Zhang et al., 2017).

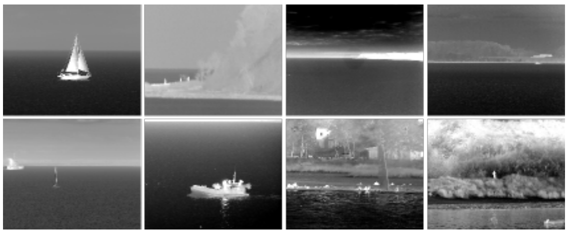

Figure 7: Sample clean images from WTD 71 test dataset.

4.1 Standard Evaluation

The results of the CNNs are evaluated with the standard peak signal-to-noise ratio (PSNR) and structural similarity (SSIM) metric and are compared with the results from a selected number of denoising and super-resolution methods publicly available for testing. Figure 8 shows the improvement of average PSNR by our denoising CNN on a batch of the validation data over each training epoch. Denoising is performed on 44 test images. Figure 9 and Figure 10 show a few denoising examples of granular noise with BM3D, PGPD, our CNN and DnCNN. The denoising CNN is not trained to denoise Gaussian noise but is tested with Gaussian noise of standard deviation (σ) of 25, to test its robustness. Figure 11 shows an example denoising result for Gaussian noise. Each of the denoising examples show selected areas inside the original image, while the PSNR values represent the entire original image. The average performance of the CNN for both granular noise and Gaussian noise is shown in Table 3. The results show that the denoising CNN is capable of performing well even without being explicitly trained for a particular kind of noise profile. The results also show that the CNN can perform well on different noise profiles without explicit manual parameter setup usually required by standard Gaussian denoisers. In other words, irrespective of the noise content in terms of the type of noise or the noise power, the CNN generalizes the denoising problem well, while other methods need prior information about the noise for good performance. Another advantage of the denoising CNN is that it does not degrade a clean image or an image with negligible noise content, when operated on, proving its robustness as well.

Similar to the denoising CNN, an improvement of the average PSNR by the super-resolution CNN on a

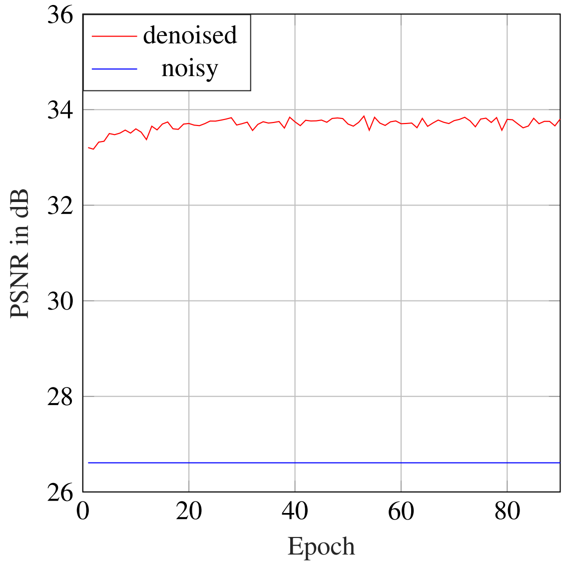

Figure 8: Comparison of average PSNR of a set of noisy and denoised validation images at every training epoch.

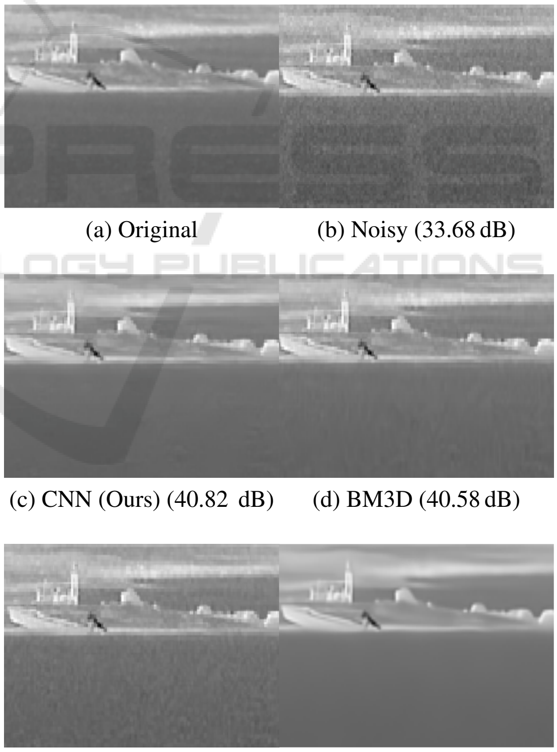

(a) Original (b) Noisy (33.68 dB)

(c) CNN (Ours) (40.82 dB) (d) BM3D (40.58 dB)

(e) PGPD (37.95 dB) (f) DnCNN (39.40 dB)

Figure 9: Denoising of granular noise in selected section in an IR image by different methods.

batch of the validation data over each training epoch, can be seen in Figure 12. For testing, super-resolution is performed on the aforementioned test images for three upsampling ratios. Figure 13 shows two exam-

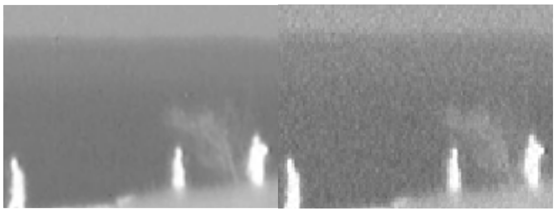

(a) Original (b) Noisy (33.19 dB)

(c) CNN (Ours) (42.33 dB) (d) BM3D (41.52 dB)

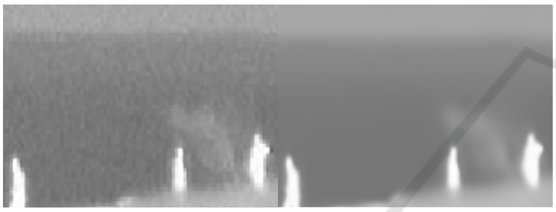

(e) PGPD (38.10 dB) (f) DnCNN (41.65 dB)

Figure 10: Denoising of granular noise in selected section in an IR image by different methods.

Table 3: Evaluation of average denoising performance (SSIM, PSNR in dB).

Method	Image Grain		Gaussian (σ = 25)	
	PSNR	SSIM	PSNR	SSIM
None	33.3	0.763	20.58	0.190
CNN	39.47	0.947	33.69	0.841
BM3D	39.42	0.942	33.83	0.848
PGPD	37.47	0.901	32.94	0.802
DnCNN	38.00	0.904	33.99	0.850

ple super-resolution results and Figure 14 shows example results for multiple super-resolution factors. The performance of our super-resolution CNN is also compared with SRCNN (Dong et al., 2015), DnCNN (Zhang et al., 2017), and VDSR (Kim et al., 2016), which are some of the standard state-of-the-art super-resolution methods. The methods are applied on the WTD71 dataset and the corresponding results are tabulated in Table 4 and Table 5. Figure 15 shows an example from the application of each of these methods for a super-resolution factor of 4. The results indicate that our CNN is very competitive with respect to VDSR and DnCNN. Our super-resolution CNN also has lesser number of training parameters compared to the other deep networks.

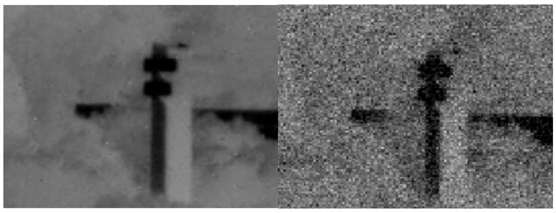

(a) Original (b) Noisy (20.93 dB)

(c) CNN (Ours) (33.29 dB) (d) BM3D (32.07 dB)

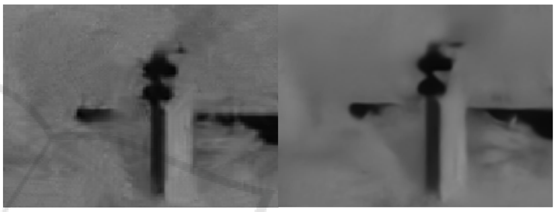

(e) PGPD (31.95 dB) (f) DnCNN (32.05 dB)

Figure 11: Denoising of Gaussian noise (σ=25) in selected section in an IR image by different methods.

Table 4: Comparison of super-resolution performance (PSNR).

Method	PSNR (dB)		
	×2	×3	×4
Bicubic	37.25	34.75	33.29
CNN (ours)	39.21	36.15	34.45
SRCNN	38.76	35.91	34.17
VDSR	39.22	36.20	34.54
DnCNN	38.79	36.02	34.45

Table 5: Comparison of super-resolution performance (SSIM).

Method	SSIM		
	×2	×3	×4
Bicubic	0.92	0.87	0.84
CNN (ours)	0.94	0.90	0.87
SRCNN	0.94	0.89	0.86
VDSR	0.94	0.90	0.88
DnCNN	0.93	0.88	0.85

4.2 Blind Denoising

In real world images, prior knowledge of the degradation is unknown. In this context the test IR images can only be subjectively evaluated and the improve-

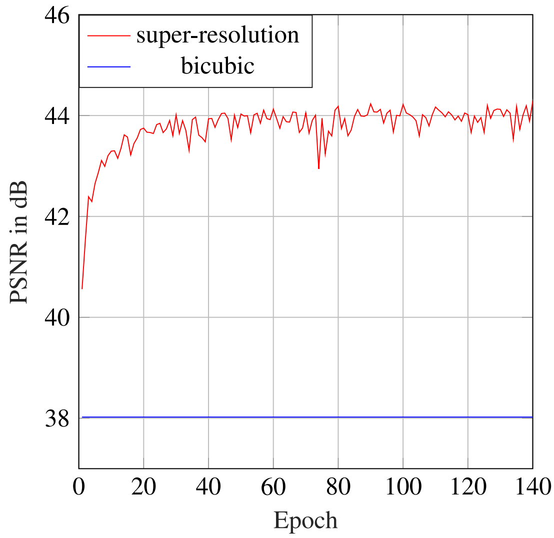

Figure 12: Comparison of average PSNR of a set of bicubic and super-resolved (×2) validation images at every training epoch.

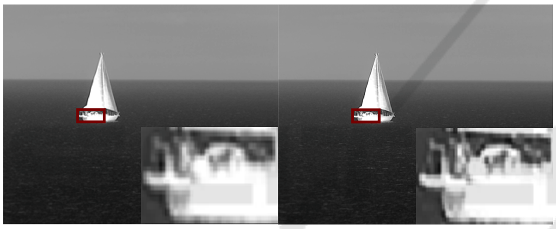

(a) Bicubic (36.06 dB) (b) CNN (Ours) (38.64 dB)

(c) Bicubic (35.07 dB) (d) CNN (Ours) (37.68 dB)

Figure 13: Comparison between bicubic interpolation and super-resolution (×2) of selected IR images.

ment can be compared through observation. The test images comprise of 20 IR images corrupted by natural artefacts. A selection of the original and denoised image sections are shown in Figure 16. From the example images it can be observed that the images contain noise artefacts and the intensity of noise is not very high. The images are a collection of frames from specific videos and have the appearance of graininess and repetitive patterns. Areas from the original images and the processed versions of the images in Figure 16 show the denoising performance of the CNN. From the images it can be observed that the graininess

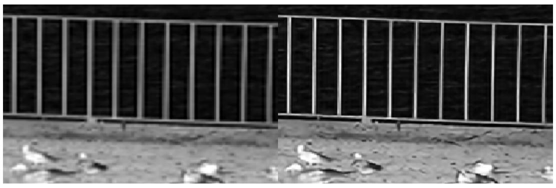

(a) Bicubic (23.78 dB) (b) CNN (Ours) (26.73 dB)

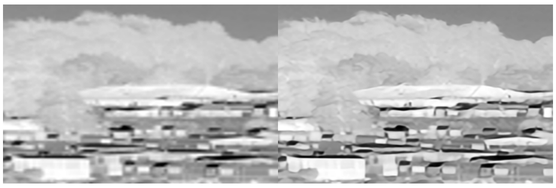

(c) Bicubic (24.60 dB) (d) CNN (Ours) (25.78 dB)

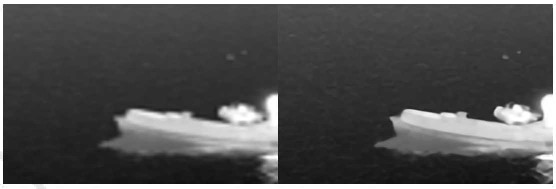

(e) Bicubic (29.97 dB) (f) CNN (Ours) (31.28 dB)

Figure 14: Comparison between (a) bicubic and (b) super-resolution (×2) (c) bicubic and (d) super-resolution (×3) and (e) bicubic and (f) super-resolution (×4) of selected sections of IR images.

(a) Original (b) Bicubic (35.07 dB)

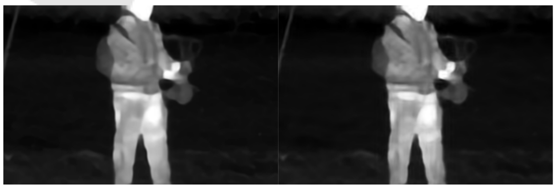

(c) CNN (Ours) (38.27 dB) (d) SRCNN (37.75 dB)

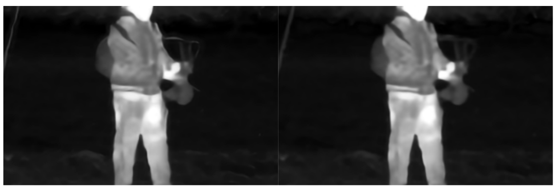

(e) VDSR (38.11 dB) (f) DnCNN (38.06 dB)

Figure 15: Super-resolution (×4) of a selected section in an IR image by different super-resolution methods.

Figure 16: Example of denoising of natural images with original image areas shown in the left column and the corresponding denoised areas shown in the right column (best observed on a monitor).

of the images is reduced while preserving the edges considerably well. The differences are best observed on a monitor.

5 CONCLUSION

In this paper we have proposed image enhancement approaches for maritime IR images. We use two CNNs with residual architectures based on regression losses to denoise and super-resolve IR images. The training images are created by adding noise content in clean images. From the objective and subjective evaluation based on example images it can be concluded that the denoising and super-resolution performs well with our networks. The results show that the CNNs are able to improve the quality of IR images. The results also encourage further investigation of simple CNN structures and improving their robustness to different types of noise, different intensities of noise and different grain sizes since the present network is limited to the data it is trained with. Further investigation can be made on the training data requirement, e.g., training with thermal images only, for better domain specific learning. It is also noteworthy that other vision tasks like segmentation, detection, and stabilization also benefit from the enhancement of images and the influence can be investigated in the future.

REFERENCES

Brown, M. and Süsstrunk, S. (2011). Multispectral SIFT for scene category recognition. In *Computer Vision and Pattern Recognition (CVPR11), 177-184*, Colorado Springs. IEEE.

doi:10.1109/CVPR.2011.5995637. Retrieved from http://ivrl.epfl.ch/supplementary_material/cvpr11/.

Burger, H. C., Schuler, C. J., and Harmeling, S. (2012). Image denoising: Can plain neural networks compete with BM3D? In *IEEE Conference on Computer Vision and Pattern Recognition, 2392-2399*. IEEE. doi: 10.1109/CVPR.2012.6247952.

Dabov, K., Foi, A., Katkovnik, V., and Egiazarian, K. (2007). Image denoising by sparse 3-d transform-domain collaborative filtering. In *IEEE Transactions on Image Processing, 16(8), 2080-2095*. IEEE. doi:10.1109/TIP.2007.901238.

Dong, C., Loy, C. C., He, K., and Tang, X. (2015). Image super-resolution using deep convolutional networks. In *IEEE Transactions on Pattern Analysis and Machine Intelligence, 38(2), 295-307*. IEEE. doi:10.1109/TPAMI.2015.2439281.

Elad, M. and Aharon, M. (2006). Image denoising via learned dictionaries and sparse representation. In *IEEE Computer Society Conference on Computer Vision and Pattern Recognition (CVPR), 1, 895-900*. IEEE. doi:10.1109/CVPR.2006.142.

Glorot, X. and Bengio, Y. (2010). Understanding the difficulty of training deep feedforward neural networks. In *Proceedings of the Thirteenth International Conference on Artificial Intelligence and Statistics, 9, 249-256*. JMLR. Retrieved from http://proceedings.mlr.press/v9/glorot10a.html.

Goldstein, T. and Osher, S. (2009). The split bregman method for L1 regularized problems. In *SIAM Journal on Imaging Sciences, 2(2), 323-343*. Society for Industrial and Applied Mathematics Philadelphia. doi:10.1137/080725891.

He, K., Zhang, X., Ren, S., and Sun, J. (2016). Deep residual learning for image recognition. In *IEEE Conference on Computer Vision and Pattern Recognition (CVPR), 770-778*. IEEE. doi:10.1109/CVPR.2016.90.

Jain, V. and Seung, S. (2009). Natural image denoising with convolutional networks. In *Advances in Neural Information Processing Systems 21, 769-776*. Curran Associates, Inc. Retrieved from http://papers.nips.cc/paper/3506-natural-image-denoising-with-convolutional-networks.pdf.

J.Xu, L.Zhang, Zuo, W., Zhang, D., and Feng, X. (2015). Patch group based nonlocal self-similarity prior learning for image denoising. In *IEEE International Conference on Computer Vision (ICCV), 244-252*. IEEE. doi:10.1109/ICCV.2015.36.

Kim, J., Lee, J. K., and Lee, K. M. (2016). Accurate image super-resolution using very deep convolutional networks. In *IEEE Computer Society Conference on Computer Vision and Pattern Recognition (CVPR), 1646-1654*. IEEE. doi:10.1109/CVPR.2016.182.

Kingma, D. P. and Ba, J. (2014). Adam: A method for stochastic optimization. In *3rd International Conference for Learning Representations*. CoRR. Retrieved from http://arxiv.org/abs/1412.6980.

Micchelli, C. A., Shen, L., and Y.Xu (2011). Proximity algorithms for image models: denoising. In *Inverse Problems, 27(4)*. Retrieved from http://stacks.iop.org/0266-5611/27/i=4/a=045009.

Pan, T., Zhongliang, F., Lili, W., and Kai, Z. (2016). Perceptual loss with fully convolutional for image residual denoising. In *T. Tan et al. (eds.) Chinese Conference on Pattern Recognition (CCPR), 122-132*. Springer. Retrieved from https://doi.org/10.1007/978-981-10-3005-5_11.

Vedaldi, A. and Lenc, K. (2015). Matconvnet: Convolutional neural networks for matlab. In *Proceedings of the 23rd ACM international conference on Multimedia*. CoRR. Retrieved from http://arxiv.org/abs/1412.4564.

Zhang, K., Zuo, W., Chen, Y., Meng, D., and Zhang, L. (2017). Beyond a gaussian denoiser: Residual learning of deep cnn for image denoising. In *IEEE Transactions on Image Processing, 26(7), 3142-3155*. IEEE. doi:10.1109/TIP.2017.2662206.

Zhang, Z. M., Tsai, B. K., and G.Machin (2010). *Radiometric Temperature Measurements*. Elsevier, 1st edition.

Zhou, Z., Cao, J., and Liu, W. (2009). Contourlet-based image denoising algorithm using adaptive windows. In *4th IEEE Conference on Industrial Electronics and Applications (ICIEA), 3654-3657*. IEEE. doi:10.1109/ICIEA.2009.5138888.